

Supporting Information

The effect of cation size on hydride-ion conduction in $Ln\text{SrLiH}_2\text{O}_2$ ($Ln = \text{La, Pr, Nd, Sm, Gd}$) oxyhydrides

Naoki Matsui,^a Yoyo Hinuma,^{a,b} Yuki Iwasaki,^c Kota Suzuki,^{a,c} Jiang Guangzhong,^a Haq Nawaz,^{d,e} Yumiko Imai,^d Masao Yonemura,^f Masaaki Hirayama,^{a,c} Genki Kobayashi^{d,e} and Ryoji Kanno^{a,c,*}

a. All-Solid-State Battery Unit, Institute of Innovative Research, Tokyo Institute of Technology, 4259 Nagatsuta, Midori-ku, Yokohama 226-8503, Japan.

b. Center for Frontier Science, Chiba University, 1-33 Yayoi-cho, Inage, Chiba 263-8522, Japan.

c. Department of Chemical Science and Engineering, School of Materials and Chemical Technology, Tokyo Institute of Technology, 4259 Nagatsuta, Midori-ku, Yokohama 226-8502, Japan.

d. Department of Materials Molecular Science, Institute for Molecular Science, National Institute of Natural Sciences, 38 Nishigonaka, Myodaiji, Okazaki, Aichi, 444-8585, Japan.

e. SOKENDAI (The Graduate University for Advanced Studies), 38 Nishigonaka, Myodaiji, Okazaki, Aichi, 444-8585, Japan.

f. Neutron Science Laboratory (KENS), Institute of Materials Structure Science, High Energy Accelerator Research Organization (KEK), 1-1 Oho, Tsukuba, Ibaraki 305-0801, Japan.

*E-mail: kanno@echem.titech.ac.jp

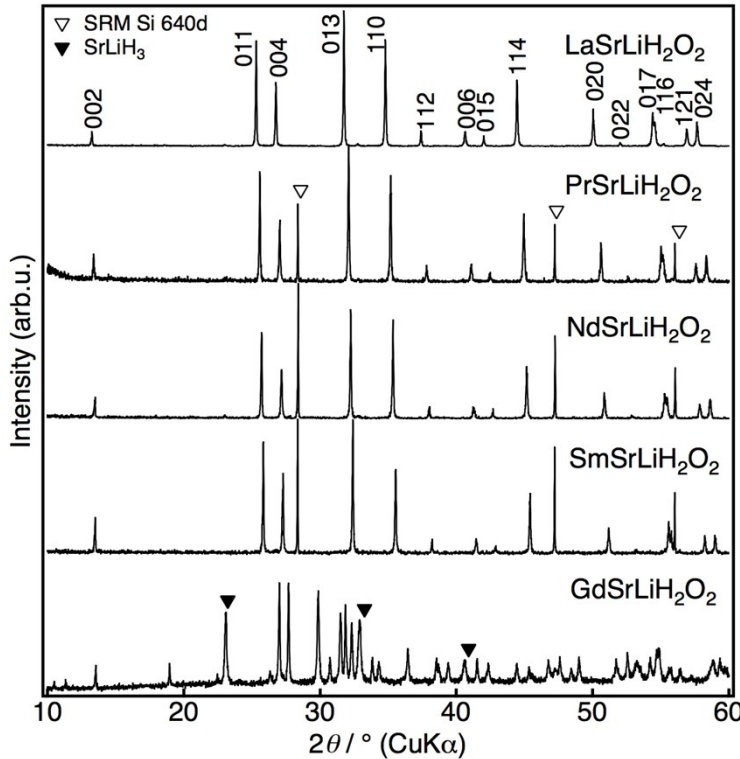


Figure S1. XRD patterns of $Ln\text{SrLiH}_2\text{O}_2$ synthesized at ambient pressure.

Supplementary note SN1. Calculation of the ionic radius of hydride ion

This section describes the method to calculate the ionic radius of the hydride ion (r_H) shown in Table 1. At first, we collected the lattice volume of metal hydride $V(M_mH_n)$ and metal fluoride $V(M_mF_n)$ from ICSD. The volumetric ratio of metal hydride to metal fluoride was defined as $V_{HF} = V(M_mH_n)/V(M_mF_n)$. V_{HF} was plotted against the difference in Pauling electronegativity between hydrogen and surrounding cations ($\Delta\chi$), as shown in Fig. S2.¹ An average value of electronegativity for Ln , Sr, and Li was used as the electronegativity of a virtual cation ($Ln_{1/3}\text{Sr}_{1/3}\text{Li}_{1/3}$). H⁻ is coordinated by two Ln , two Sr, and two Li in $Ln\text{SrLiH}_2\text{O}_2$, therefore the virtual cation is a simple average of the three cation species. Based on the linear fitting, the relational expression of the volumetric ratio was calculated as; $V_{HF} = 1.02 \times \Delta\chi - 0.23$. The average electronegativity of cation, $\Delta\chi$, and V_{HF} for $Ln\text{SrLiH}_2\text{O}_2$ are listed in Table S1. Finally,

$$r_H = r_M \left(V_{HF}^{\frac{1}{3}} - 1 \right) + r_F V_{HF}^{\frac{1}{3}}$$

the ionic radius of H⁻ was calculated using $r_H = r_M \left(V_{HF}^{\frac{1}{3}} - 1 \right) + r_F V_{HF}^{\frac{1}{3}}$, where r_M and r_F are the ionic radius of cation and fluoride ion (1.4 Å), respectively.¹

Table S1. The parameters used in the calculation of the ionic radius of hydride ion.

Composition	electronegativity of virtual cation ($Ln_{1/3}Sr_{1/3}Li_{1/3}$)	$\Delta\chi$	V_{HF}	$r_H / \text{\AA}$
LaSrLiH ₂ O ₂	1.01	1.19	0.98	1.32
PrSrLiH ₂ O ₂	1.02	1.18	0.97	1.31
NdSrLiH ₂ O ₂	1.02	1.18	0.97	1.31
SmSrLiH ₂ O ₂	1.03	1.17	0.96	1.30
GdSrLiH ₂ O ₂	1.04	1.16	0.95	1.29
TbSrLiH ₂ O ₂	1.05	1.15	0.95	1.29

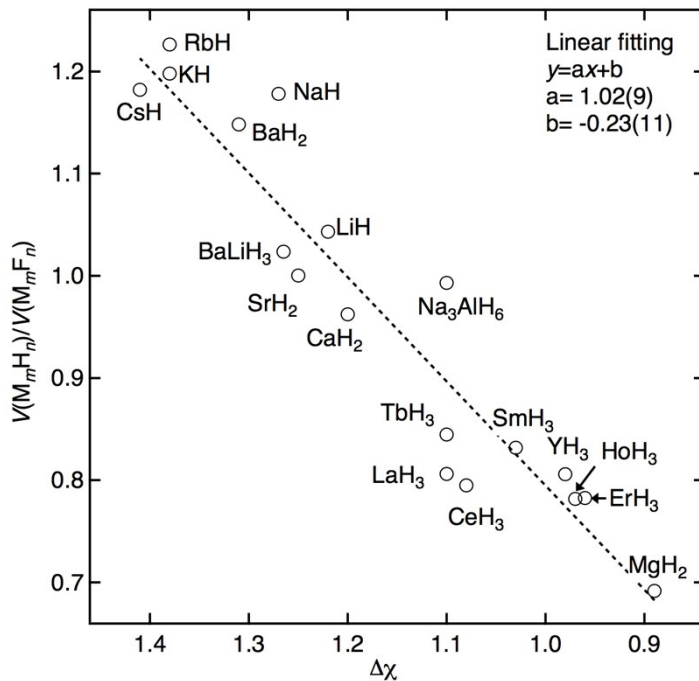


Figure S2. The relationship between the volumetric metal hydride-to-metal fluoride ratio and the difference in Pauling electronegativity between metal and hydrogen ($\Delta\chi$).¹ The ionic radius of hydride ion was calculated based on $\Delta\chi$ and the ionic radius of fluoride ion (1.4 Å).

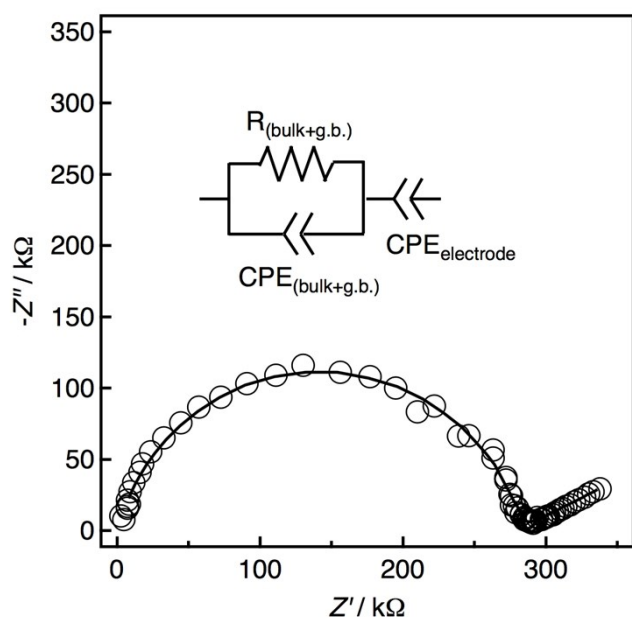


Figure S3. Impedance plot of NdSrLiH₂O₂ (high-pressure synthesis) measured at 260 °C. Observed data points and the fitting curve are indicated by the circles and solid line, respectively. The equivalent circuit used for fitting the semicircle and spike is shown in the inset.

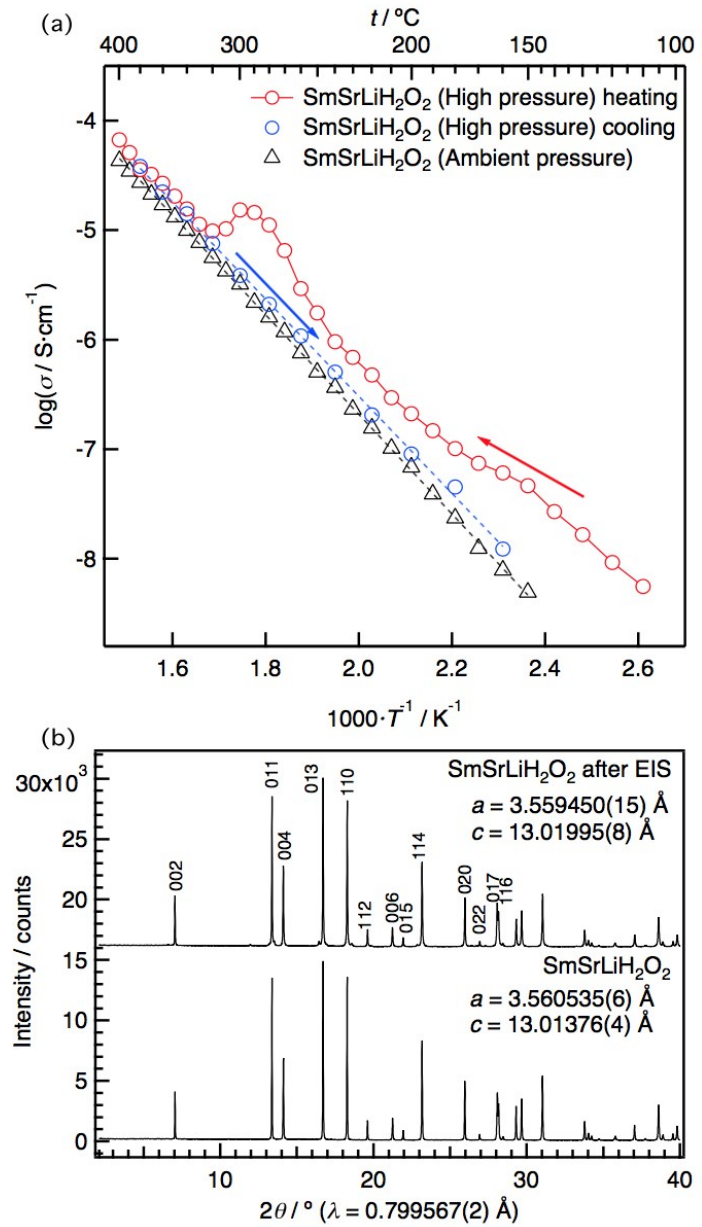


Figure S4. (a) Arrhenius plots of $\text{SmSrLiH}_2\text{O}_2$ during heating and cooling. (b) Synchrotron XRD patterns of $\text{SmSrLiH}_2\text{O}_2$ before and after electrochemical impedance spectroscopy (EIS) measurements. The lattice parameters corresponding to the indicated diffraction patterns are included.

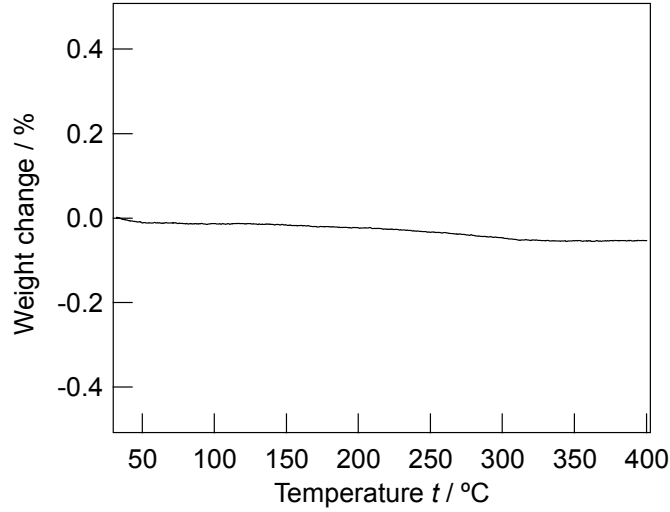


Figure S5. TG spectrum of $\text{GdSrLiH}_2\text{O}_2$ under dry Ar flow.

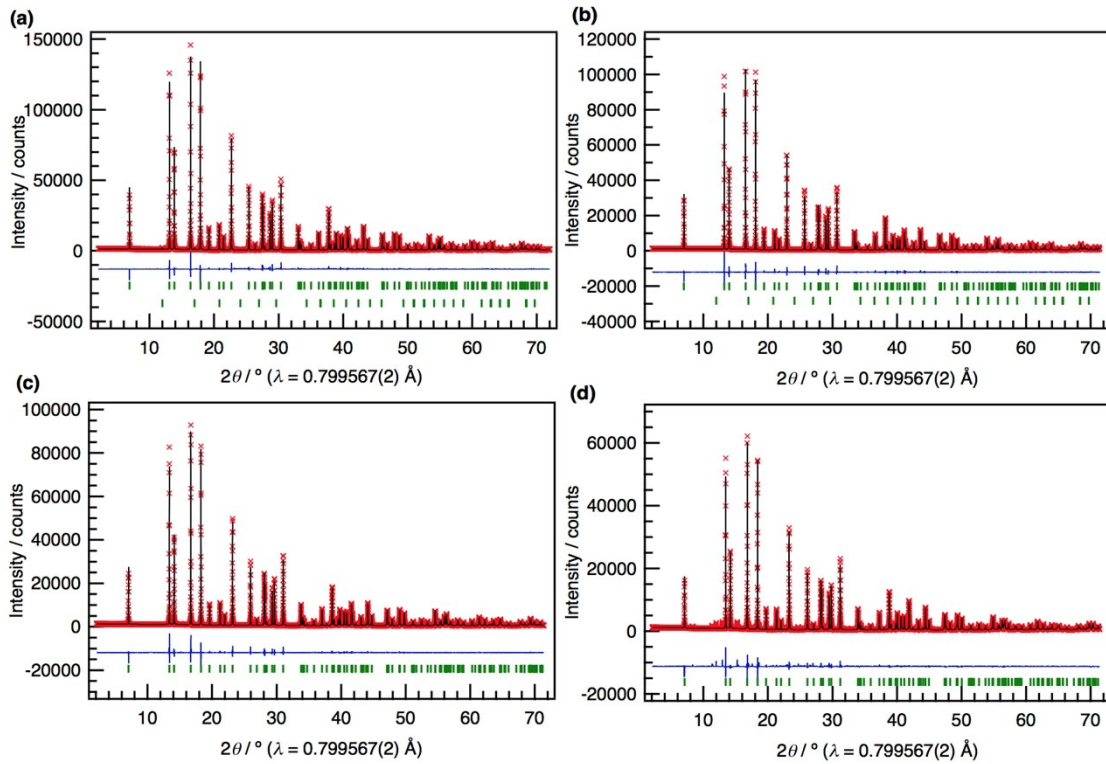


Figure S6. Rietveld refinement patterns of synchrotron X-ray diffraction data at 293 K of (a) $\text{LaSrLiH}_2\text{O}_2$, (b) $\text{PrSrLiH}_2\text{O}_2$, (c) $\text{SmSrLiH}_2\text{O}_2$, and (d) $\text{GdSrLiH}_2\text{O}_2$, each synthesized under high pressure. Red crosses: observed intensities; solid black line: calculated intensities; solid blue line: difference curve. The upper and lower green markers indicate the positions of the diffraction lines of $\text{LnSrLiH}_2\text{O}_2$ and SrLiH_3 , respectively.

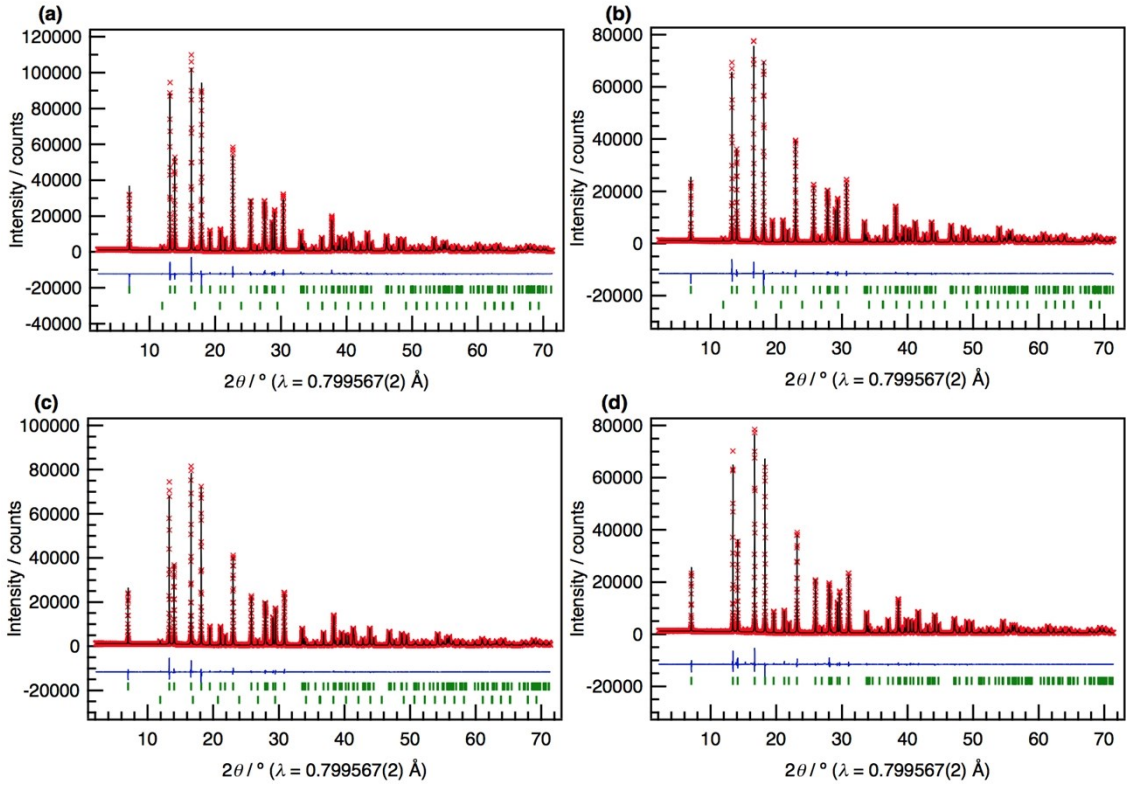


Figure S7. Rietveld refinement patterns of synchrotron X-ray diffraction data at 293 K of (a) LaSrLiH₂O₂, (b) PrSrLiH₂O₂, (c) NdSrLiH₂O₂, and (d) SmSrLiH₂O₂, each synthesized under ambient pressure. Red crosses: observed intensities; solid black line: calculated intensities; solid blue line: difference curve. The upper and lower green makers indicate the positions of the diffraction lines of Ln SrLiH₂O₂ and SrLiH₃, respectively.

Table S2. Rietveld refinement results from the synchrotron X-ray diffraction data of LaSrLiH₂O₂ synthesized under high pressure.

Atom	Site	<i>g</i>	<i>x</i>	<i>y</i>	<i>z</i>	<i>U</i> _{iso} / Å ²
La ³⁺	4e	0.5	0	0	0.35623(2)	0.00420(4)
Sr ²⁺	4e	0.5	0	0	= <i>z</i> (La ³⁺)	= <i>U</i> _{iso} (La ³⁺)
Li ⁺	2a	1	0.0	0	0	0.013
H ⁻	4c	1	0	0.5	0	0.019
O ²⁻	4e	1	0	0	0.17054(13)	0.0127(5)

Unit cell: tetragonal *I*4/*mmm* (139); *a* = *b* = 3.638971(5) Å, *c* = 13.28876(3) Å, *V* = 175.971 Å³; *R*_{wp} = 6.43%, *R*_p = 4.73%, *R*_F = 2.07%, *S* = 2.67; secondary phase: SrLiH₃ (~3.3 mass%).

Table S3. Rietveld refinement results from the synchrotron X-ray diffraction data of PrSrLiH₂O₂ synthesized under high pressure.

Atom	Site	<i>g</i>	<i>x</i>	<i>y</i>	<i>z</i>	<i>U</i> _{iso} / Å ²
Pr ³⁺	4e	0.5	0	0	0.35597(2)	0.00401(5)
Sr ²⁺	4e	0.5	0	0	= <i>z</i> (Pr ³⁺)	= <i>U</i> _{iso} (Pr ³⁺)
Li ⁺	2a	1	0.0	0	0	0.013
H ⁻	4c	1	0	0.5	0	0.019
O ²⁻	4e	1	0	0	0.17102(17)	0.0146(6)

Unit cell: tetragonal *I*4/*mmm* (139); *a* = *b* = 3.599600(7) Å, *c* = 13.14087(5) Å, *V* = 170.268 Å³; *R*_{wp} = 7.53%, *R*_p = 5.28%, *R*_F = 1.52%, *S* = 2.90; secondary phase: SrLiH₃ (~1.1 mass%).

Table S4. Rietveld refinement results from the synchrotron X-ray diffraction data of NdSrLiH₂O₂ synthesized under high pressure.

Atom	Site	<i>g</i>	<i>x</i>	<i>y</i>	<i>z</i>	<i>U</i> _{iso} / Å ²
Nd ³⁺	4e	0.5	0	0	0.35591(2)	0.00345(4)
Sr ²⁺	4e	0.5	0	0	= <i>z</i> (Nd ³⁺)	= <i>U</i> _{iso} (Nd ³⁺)
Li ⁺	2a	1	0.0	0	0	0.013
H ⁻	4c	1	0	0.5	0	0.019
O ²⁻	4e	1	0	0	0.17113(12)	0.0151(4)

Unit cell: tetragonal *I*4/*mmm* (139); *a* = *b* = 3.585637(5) Å, *c* = 13.09739(3) Å, *V* = 168.390 Å³; *R*_{wp} = 5.38%, *R*_p = 4.00%, *R*_F = 1.32%, *S* = 2.08; secondary phase: SrLiH₃ (~3.9 mass%).

Table S5. Rietveld refinement results from the synchrotron X-ray diffraction data of SmSrLiH₂O₂ synthesized under high pressure.

Atom	Site	<i>g</i>	<i>x</i>	<i>y</i>	<i>z</i>	<i>U</i> _{iso} / Å ²
Sm ³⁺	4e	0.5	0	0	0.35564(2)	0.00399(4)
Sr ²⁺	4e	0.5	0	0	= <i>z</i> (Sm ³⁺)	= <i>U</i> _{iso} (Sm ³⁺)
Li ⁺	2a	1	0.0	0	0	0.013
H ⁻	4c	1	0	0.5	0	0.019
O ²⁻	4e	1	0	0	0.17085(15)	0.0164(5)

Unit cell: tetragonal *I*4/*mmm* (139); *a* = *b* = 3.560535(6) Å, *c* = 13.01376(4) Å, *V* = 164.981 Å³; *R*_{wp} = 5.84%, *R*_p = 4.44%, *R*_F = 1.33%, *S* = 2.62.

Table S6. Rietveld refinement results from the synchrotron X-ray diffraction data of GdSrLiH₂O₂ synthesized under high pressure.

Atom	Site	<i>g</i>	<i>x</i>	<i>y</i>	<i>z</i>	<i>U</i> _{iso} / Å ²
Gd ³⁺	4e	0.5	0	0	0.3539796(12)	0.00451(7)
Sr ²⁺	4e	0.5	0	0	= <i>z</i> (Gd ³⁺)	= <i>U</i> _{iso} (Gd ³⁺)
Li ⁺	2a	1	0.0	0	0	0.013
H ⁻	4c	1	0	0.5	0	0.019
O ²⁻	4e	1	0	0	0.1704(3)	0.0172(10)

Unit cell: tetragonal *I*4/*mmm* (139); *a* = *b* = 3.539796(12) Å, *c* = 12.96940(7) Å, *V* = 162.509 Å³; *R*_{wp} = 10.21%, *R*_p = 6.29%, *R*_F = 2.99%, *S* = 3.46.

Table S7. Rietveld refinement results from the synchrotron X-ray diffraction data of LaSrLiH₂O₂ synthesized under ambient pressure.

Atom	Site	<i>g</i>	<i>x</i>	<i>y</i>	<i>z</i>	<i>U</i> _{iso} / Å ²
La ³⁺	4e	0.5	0	0	0.35619(2)	0.00341(4)
Sr ²⁺	4e	0.5	0	0	= <i>z</i> (La ³⁺)	= <i>U</i> _{iso} (La ³⁺)
Li ⁺	2a	1	0.0	0	0	0.013
H ⁻	4c	1	0	0.5	0	0.019
O ²⁻	4e	1	0	0	0.17088(13)	0.0133(5)

Unit cell: tetragonal *I*4/*mmm* (139); *a* = *b* = 3.636478(8) Å, *c* = 13.28892(4) Å, *V* = 175.732 Å³; *R*_{wp} = 5.98%, *R*_p = 4.46%, *R*_F = 1.66%, *S* = 2.40; secondary phase: SrLiH₃ (~10.2 mass%).

Table S8. Rietveld refinement results from the synchrotron X-ray diffraction data of PrSrLiH₂O₂ synthesized under ambient pressure.

Atom	Site	<i>g</i>	<i>x</i>	<i>y</i>	<i>z</i>	<i>U</i> _{iso} / Å ²
Pr ³⁺	4e	0.5	0	0	0.35588(2)	0.00313(4)
Sr ²⁺	4e	0.5	0	0	= <i>z</i> (Pr ³⁺)	= <i>U</i> _{iso} (Pr ³⁺)
Li ⁺	2a	1	0.0	0	0	0.013
H ⁻	4c	1	0	0.5	0	0.019
O ²⁻	4e	1	0	0	0.17108(15)	0.0134(6)

Unit cell: tetragonal *I*4/*mmm* (139); *a* = *b* = 3.597025(9) Å, *c* = 13.14663(5) Å, *V* = 170.099 Å³; *R*_{wp} = 6.36%, *R*_p = 4.44%, *R*_F = 1.52%, *S* = 2.39; secondary phase: SrLiH₃ (~1.8 mass%).

Table S9. Rietveld refinement results from the synchrotron X-ray diffraction data of $\text{NdSrLiH}_2\text{O}_2$ synthesized under ambient pressure.

Atom	Site	<i>g</i>	<i>x</i>	<i>y</i>	<i>z</i>	$U_{\text{iso}} / \text{\AA}^2$
Nd^{3+}	$4e$	0.5	0	0	0.355583(2)	0.00327(4)
Sr^{2+}	$4e$	0.5	0	0	$=z(\text{Nd}^{3+})$	$=U_{\text{iso}}(\text{Nd}^{3+})$
Li^+	$2a$	1	0.0	0	0	0.013
H^-	$4c$	1	0	0.5	0	0.019
O^{2-}	$4e$	1	0	0	0.17074(13)	0.0135(5)

Unit cell: tetragonal $I4/mmm$ (139); $a = b = 3.582499(7) \text{ \AA}$, $c = 13.09555(4) \text{ \AA}$, $V = 168.072 \text{ \AA}^3$;
 $R_{\text{wp}} = 5.57\%$, $R_{\text{p}} = 4.03\%$, $R_{\text{F}} = 1.35\%$, $S = 2.08$; secondary phase: SrLiH_3 (~ 6.3 mass%).

Table S10. Rietveld refinement results from the synchrotron X-ray diffraction data of $\text{SmSrLiH}_2\text{O}_2$ synthesized under ambient pressure.

Atom	Site	<i>g</i>	<i>x</i>	<i>y</i>	<i>z</i>	$U_{\text{iso}} / \text{\AA}^2$
Sm^{3+}	$4e$	0.5	0	0	0.355536(2)	0.00340(4)
Sr^{2+}	$4e$	0.5	0	0	$=z(\text{Sm}^{3+})$	$=U_{\text{iso}}(\text{Sm}^{3+})$
Li^+	$2a$	1	0.0	0	0	0.013
H^-	$4c$	1	0	0.5	0	0.019
O^{2-}	$4e$	1	0	0	0.17071(15)	0.0134(6)

Unit cell: tetragonal $I4/mmm$ (139); $a = b = 3.559394(8) \text{ \AA}$, $c = 13.03098(5) \text{ \AA}$, $V = 165.093 \text{ \AA}^3$;
 $R_{\text{wp}} = 6.71\%$, $R_{\text{p}} = 4.70\%$, $R_{\text{F}} = 1.88\%$, $S = 2.44$.

Supplementary note SN2. Derivation of the critical radius.

Figure S8 shows the geometry of atoms near the saddle point in a K_2NiF_4 -type host structure.² Focusing on triangle $A_1\text{-}A'\text{-}P$,

$$(PA')^2 + (A'A_1)^2 = (A_1P)^2 \quad \dots (\text{A1})$$

Here, A_1 and A_2 are centers of A-site cations, B is the center of the B-site cation, and P is the origin of the critical radius r_c . Using the lattice parameter c_0 , coordinate z of the A-site cation, and r_c , substituting $A'A_1 = c_0(0.5 - z)$ and $A_1P = r_A + r_c$ yields

$$PA' = \sqrt{(r_A + r_c)^2 - c_0^2(0.5 - z)^2} \quad \dots (\text{A2})$$

PA' can also be written using the lattice parameter a_0 , the radius of the B-site cation r_B , and r_c as

$$PA' + r_B + r_c = \frac{a_0}{\sqrt{2}} \quad \dots (\text{A3})$$

Substituting equation (A2) into equation (A3) yields

$$r_B + r_c + \sqrt{(r_A + r_c)^2 - c_0^2(0.5 - z)^2} = \frac{a_0}{\sqrt{2}} \quad \dots (\text{A4})$$

that can be summarized as

$$r_c = \frac{a_0 \left(\frac{a_0}{2} - \sqrt{2}r_B \right) + c_0^2(0.5 - z)^2 - (r_A + r_B)(r_A - r_B)}{2(r_A - r_B) + \sqrt{2}a_0} \quad \dots (\text{A5})$$

Note that equation (A5) is valid for this particular geometry only. The general form of r_c , where the three atoms constituting the bottleneck have different radii and the triangle is scalene, would be very complicated. Therefore, the bottleneck area (area of the triangle) is generally more convenient.

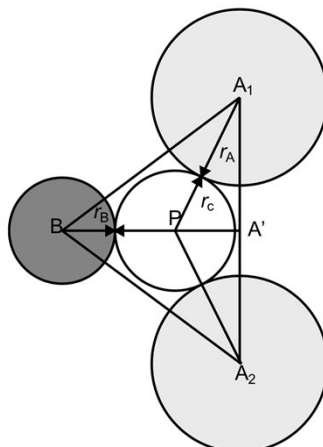


Figure S8. The critical radius r_c of the hydride ion in a K_2NiF_4 -type host.

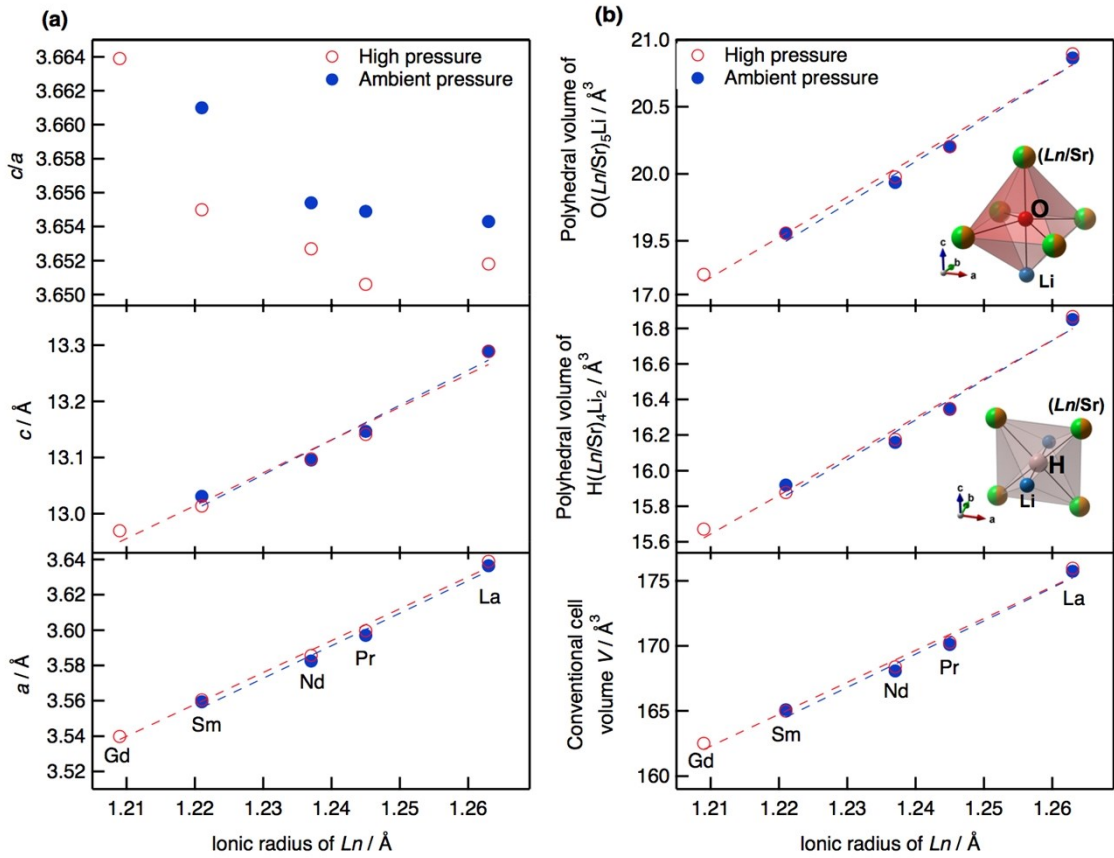


Figure S9. (a) Lattice parameters a (bottom), c (middle), and c/a ratio (top) and (b) conventional cell volume (bottom), polyhedral volume of H-centered $\text{H}(\text{Ln/Sr})_4\text{Li}_2$ octahedra (middle), and polyhedral volume of O-centered $\text{O}(\text{Ln/Sr})_5\text{Li}$ octahedra (top) of $\text{LnSrLiH}_2\text{O}_2$ as a function of lanthanide ion radius.

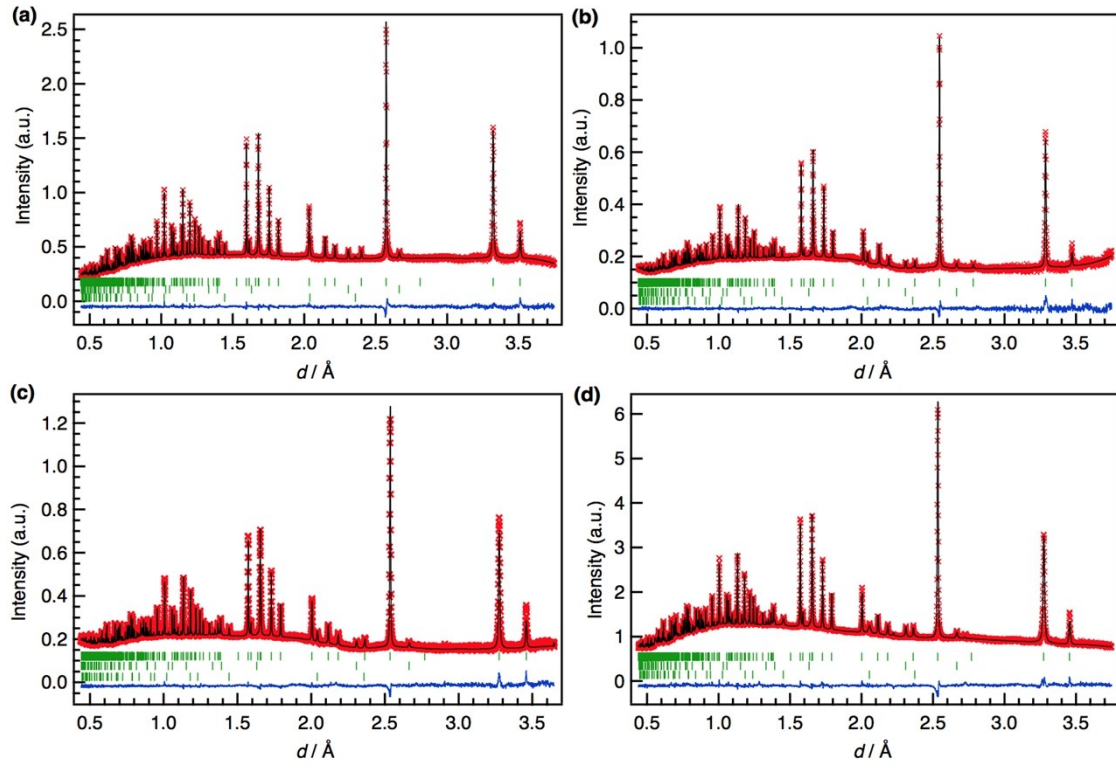


Figure S10. Rietveld refinement patterns of neutron powder diffraction data at 298 K for (a) $\text{LaSrLiH}_2\text{O}_2$, (b) $\text{PrSrLiH}_2\text{O}_2$, and (c) $\text{NdSrLiH}_2\text{O}_2$, each synthesized under high pressure, and (d) $\text{NdSrLiH}_2\text{O}_2$ synthesized under ambient pressure. Red crosses: observed intensities; solid black line: calculated intensities; solid blue line: difference curve. The green makers indicate the positions of the diffraction lines of $Ln\text{SrLiH}_2\text{O}_2$ and of LiH and SrLiH_3 impurities from top to bottom, respectively.

Table S11. Rietveld refinement results from the neutron powder diffraction data of NdSrLiH₂O₂ synthesized under ambient pressure.

Atom	Site	<i>g</i>	<i>x</i>	<i>y</i>	<i>z</i>	<i>U</i> ₁₁ / Å ²	<i>U</i> ₂₂ / Å ²	<i>U</i> ₃₃ / Å ²	<i>U</i> _{iso} / Å ²
Nd	4e	0.5	0	0	0.35590(4)	0.00462(15)	= <i>U</i> ₁₁ [Nd]	0.0054(2)	0.0051(11)
Sr	4e	0.5	0	0	= <i>z</i> [Nd]	= <i>U</i> ₁₁ [Nd]	= <i>U</i> ₁₁ [Nd]	= <i>U</i> ₃₃ [Nd]	0.0051(11)
Li	2a	1	0	0	0	0.0028(8)	= <i>U</i> ₁₁ [Li]	0.031(2)	0.0131(8)
H(1)	4c	0.9568(12)	0	0.5	0	0.0287(11)	0.0130(8)	0.0116(10)	0.0187(6)
O(1)	4c	=1- <i>g</i> [H(1)]	0	0.5	0	= <i>U</i> ₁₁ [H(1)]	= <i>U</i> ₂₂ [H(1)]	= <i>U</i> ₃₃ [H(1)]	= <i>U</i> _{iso} [H(1)]
O(2)	4e	0.9405(2)	0	0	0.17197(6)	0.0113(3)	= <i>U</i> ₁₁ [O(2)]	0.0048(4)	0.0085(2)
H(2)	4e	=1- <i>g</i> [O(2)]	0	0	= <i>z</i> [O(2)]	= <i>U</i> ₁₁ [O(2)]	= <i>U</i> ₁₁ [O(2)]	= <i>U</i> ₃₃ [O(2)]	= <i>U</i> _{iso} [O(2)]

Unit cell: tetragonal *I*4/*mmm* (139); *a* = *b* = 3.583599(13) Å, *c* = 13.10404(11) Å, *V* = 168.2841(14) Å³; *R*_{wp} = 1.80%, *R*_p = 1.46%,

*R*_F = 6.62%, *S* = 1.90; secondary phase: LiH (~1.9 mass%), tertiary phase: Li₂O (~1.5 mass%), quaternary phase: SrLiH₃ (~0.6 mass%).

Table S12. Calculated lattice parameters of *Ln*SrLiH₂O₂

		LaSrLiH ₂ O ₂	PrSrLiH ₂ O ₂	NdSrLiH ₂ O ₂	SmSrLiH ₂ O ₂	GdSrLiH ₂ O ₂
<i>a</i> / Å	Experimental	3.639	3.560	3.586	3.561	3.540
	Calculation	3.609	3.577	3.559	3.523	3.488
<i>c</i> / Å	Experimental	13.29	13.14	13.10	13.01	12.97
	Calculation	13.01	12.99	12.93	12.92	12.90

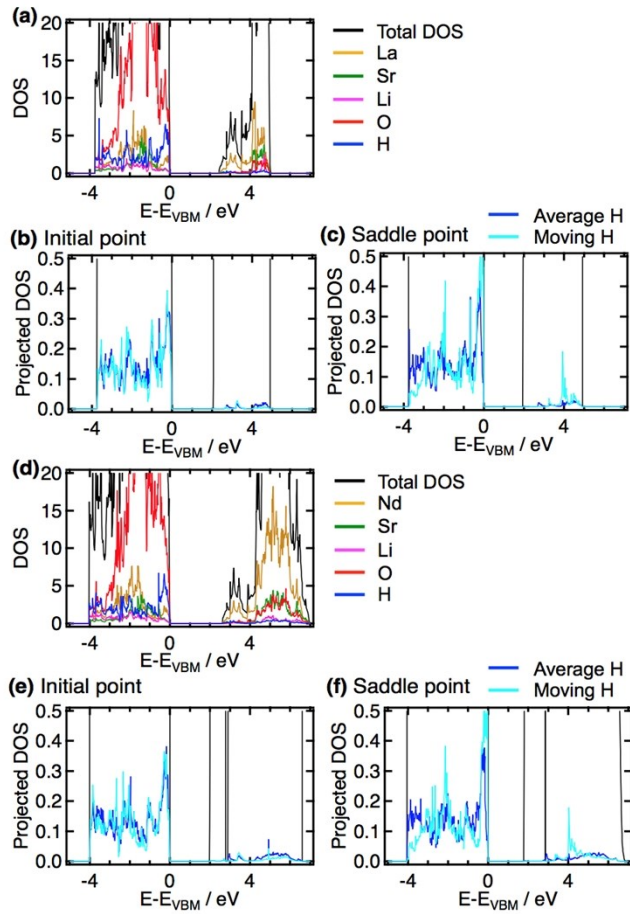


Figure S11. Density of state (DOS) plots of (a) $\text{LaSrLiH}_2\text{O}_2$ and (d) $\text{NdSrLiH}_2\text{O}_2$. Projected DOS of moving hydrogen at the (b,e) initial and (c,f) saddle points of $\text{LaSrLiH}_2\text{O}_2$ (upper) and $\text{NdSrLiH}_2\text{O}_2$ (lower).

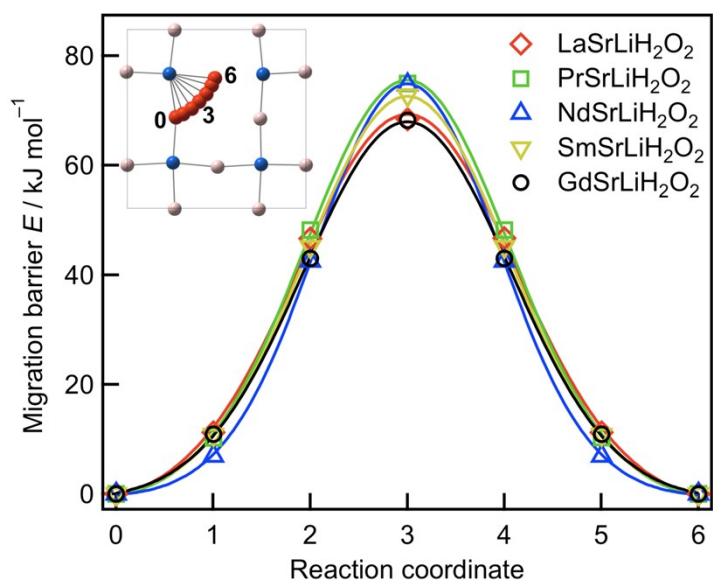


Figure S12. Migration barrier for oxide ion hopping via hydride ion vacancies in $Ln\text{SrLiH}_2\text{O}_2$. The corresponding reaction coordinate is also shown.

Reference

1. L. Pauling. The nature of the chemical bond. IV. The energy of single bonds and the relative electronegativity of atoms. *J. Am. Chem. Soc.* **1932**, 54, 3570.
2. J. A. Kilner and R. J. Brook. A study of oxygen ion conductivity in doped non-stoichiometric oxides. *Solid State Ionics* **1982**, 6, 237.